



In Vivo Optical Characterization of Middle Ear Effusions and Biofilms During Otitis Media

Jungeun Won^{1,2} · Guillermo L. Monroy² · Pawjai Khampang³ · Ronit Barkalifa² · Wenzhou Hong³ · Eric J. Chaney² · Edita Aksamitiene² · Ryan G. Porter^{4,7} · Michael A. Novak⁴ · Darold R. Spillman Jr.² · Joseph E. Kerschner^{3,5} · Stephen A. Boppart^{1,2,6,7,8}

Received: 13 March 2023 / Accepted: 15 May 2023 / Published online: 30 May 2023
© The Author(s) under exclusive licence to Association for Research in Otolaryngology 2023

Abstract

Otitis media (OM), a common ear infection, is characterized by the presence of an accumulated middle ear effusion (MEE) in a normally air-filled middle ear cavity. While assessing the MEE plays a critical role in the overall management of OM, identifying and examining the MEE is challenging with the current diagnostic tools since the MEE is located behind the semi-opaque eardrum. The objective of this cross-sectional, observational study is to non-invasively visualize and characterize MEEs and bacterial biofilms in the middle ear. A portable, handheld, otoscope-integrated optical coherence tomography (OCT) system combined with novel analytical methods has been developed. In vivo middle ear OCT images were acquired from 53 pediatric subjects (average age of 3.9 years; all awake during OCT imaging) diagnosed with OM and undergoing a surgical procedure (ear tube surgery) to aspirate the MEE and aerate the middle ear. In vivo middle ear OCT acquired prior to the surgery was compared with OCT of the freshly extracted MEEs, clinical diagnosis, and post-operative evaluations. Among the subjects who were identified with the presence of MEEs, 89.6% showed the presence of the TM-adherent biofilm in in vivo OCT. This study provides an atlas of middle ear OCT images exhibiting a range of depth-resolved MEE features, which can only be visualized and assessed non-invasively through OCT. Quantitative metrics of OCT images acquired prior to the surgery were statistically correlated with surgical evaluations of MEEs. Measurements of MEE characteristics will provide new readily available information that can lead to improved diagnosis and management strategies for the highly prevalent OM in children.

Keywords Biofilm · Middle ear effusion · Optical coherence tomography · Otitis media · Otoscopy · Imaging

Introduction

Otitis media (OM), or a middle ear infection, is a common pediatric disease caused by bacterial and/or viral pathogens associated with upper respiratory infections (URIs) [1, 2].

OM can be clinically described by the presence of a middle ear effusion (MEE), the accumulated middle ear secretion in an aerated middle ear cavity, with common symptoms of ear pain (otalgia), feeling of ear fullness, and fever. The prolonged presence of the MEE can obstruct the middle ear

✉ Stephen A. Boppart
boppart@illinois.edu

¹ Department of Bioengineering, University of Illinois Urbana-Champaign, Urbana, IL 61801, USA

² Beckman Institute for Advanced Science and Technology, 405 N Mathews Ave, Urbana, IL 61801, USA

³ Department of Otolaryngology and Communication Sciences, Medical College of Wisconsin, Milwaukee, WI 53226, USA

⁴ Department of Otolaryngology, Carle Foundation Hospital, Urbana, IL 61801, USA

⁵ Division of Otolaryngology and Pediatric Otolaryngology, Medical College of Wisconsin, Milwaukee, WI 53226, USA

⁶ Department of Electrical and Computer Engineering, University of Illinois Urbana-Champaign, Urbana, IL 61801, USA

⁷ Carle Illinois College of Medicine, University of Illinois Urbana-Champaign, Urbana, IL 61801, USA

⁸ NIH/NIBIB P41 Center for Label-free Imaging and Multiscale Biophotonics (CLIMB), University of Illinois Urbana-Champaign, Urbana, IL 61801, USA

vibratory system, leading to conductive hearing loss, which may negatively impact speech and language development in children. Primary treatment strategies include antibiotic prescription for acute OM, and if indicated, surgical myringotomy with tympanostomy tube placement (M&T, or ear tube surgery) for chronic and recurrent OM [3]. Myringotomy creates an incision in the tympanic membrane (TM, or eardrum) to place a tympanostomy tube that can drain a persistent MEE and aerate the middle ear. Around 31% of children aged 3 to 17 years with frequent ear infections received M&T in 2014 [4]. OM has an estimated US medical expenditure of > \$4 billion annually [5, 6] and M&T as a result of OM is the leading cause of ambulatory surgery requiring a general anesthetic during childhood in the USA [7].

Assessing MEEs is a key diagnostic challenge because current middle ear diagnostic tools are limited in their ability to provide direct measurement and visualization of MEEs. The presence of a MEE behind the TM needs to be confirmed to establish a diagnosis of OM [8, 9]. MEEs can also be clinically categorized into serous (watery and clear), mucoid (mucus-containing), or purulent (pus-containing) types, and can be assessed in terms of its relative fluid volume (air-fluid level), such as scant or filling MEE. However, standard otoscopy has an overall diagnostic accuracy of 50–70%, depending on physician experience and expertise [10, 11].

To improve the diagnostic capability by non-invasively imaging the middle ear cavity, optical coherence tomography (OCT) has been proposed and investigated for its clinical utility during the past decade [12, 13]. OCT is an optical analogue of ultrasound imaging and generates depth-resolved cross-sectional images of tissue by detecting light-echoes [14] and does not require contact with the TM nor any impedance matching gel. OCT can provide multi-dimensional images at a video rate with a depth resolution of 2–10 μm . Recent studies showed that MEEs can be visualized with OCT in Pediatric, Primary Care, and Ear, Nose, and Throat (ENT) outpatient clinics [15–17] and in an operating room during M&T [18, 19], with a reported accuracy of 90.6% for detecting a MEE in pediatric patients [20]. Quantitative assessments allowed the estimation of relative viscosity [21] and fluid level, which has been correlated with the acoustic responses of the middle ear [15]. Non-invasive detection of a thin bacterial biofilm affixed to the TM during chronic OM has also been demonstrated [12, 18]. The biofilm, composed of aggregated bacteria enclosed within an adherent matrix, is thought to be responsible for ineffective antibiotic treatments, leading to the repeated episodes of OM [22, 23]. The role of biofilms as a hallmark of chronic and recurrent OM has been actively investigated [24, 25].

Though widely applied to various presentations of OM, a systematic study that correlates OCT-based features of MEEs with pre-operative and post-operative assessment to validate

its clinical feasibility has not been performed. In this study, a portable OCT system with a handheld probe has been developed to non-invasively characterize the MEEs in pediatric subjects before and after M&T. Overall, this work has two main objectives: (1) bridging optical information about the MEEs with biologically and clinically validated information and (2) expanding the OCT database of MEEs during OM, all to further translate the OCT technology to otology.

Materials and Methods

Human Subjects and Sample Collection

Investigational oversight followed an approved protocol from the Institutional Review Boards (IRBs) at both the University of Illinois Urbana-Champaign and Carle Foundation Hospital (Urbana, IL). Written informed consents and assents (if eligible) were obtained from parents/legal guardians and subjects. Pediatric subjects older than 12 months undergoing M&T with intact TM were recruited for the study from April 2019 to August 2020. Exclusion criteria were subjects with tubes present bilaterally and subjects who had M&T in the past 3 months. A total of 53 subjects (average age of 3.9 years) participated in the study.

In vivo middle ear OCT imaging and standard otoscopy were performed 1 h prior to M&T in a pre-operative room at Carle Foundation Hospital, adjacent to the surgery suite. Note that the OCT imaging was performed while the subjects were awake (before anesthesia). The handheld OCT probe resembles a standard otoscope in shape and size (Fig. 1a), and utilizes regular, disposable ear specula. Each OCT imaging session required < 10 min per subject (5 min/ear) to minimize interruption for surgery schedules. For each subject, > 40 OCT frames (B-scans) captured around the light reflex region on the TM for each ear were collected. All subjects sat on either an exam chair or a parent's lap. Two ENT specialists performed the M&T procedures, and collected the MEEs using a Juhn Tym-Tap middle ear fluid aspirator (Medtronic, Minneapolis, MN). Each extracted MEE sample was freshly imaged again shortly after in the Juhn Tym-Tap fluid container with the same OCT system that had been used to acquire in vivo middle ear OCT prior to the surgery. A photo of the gross appearance of the MEE sample was acquired under constant and consistent illumination and background, and a rough volume of the MEE sample was estimated using a graduated container. The samples were then stored at $-80\text{ }^{\circ}\text{C}$ until further testing. The pre- and post-operative reports were obtained after the study to correlate with the OCT-derived metrics.

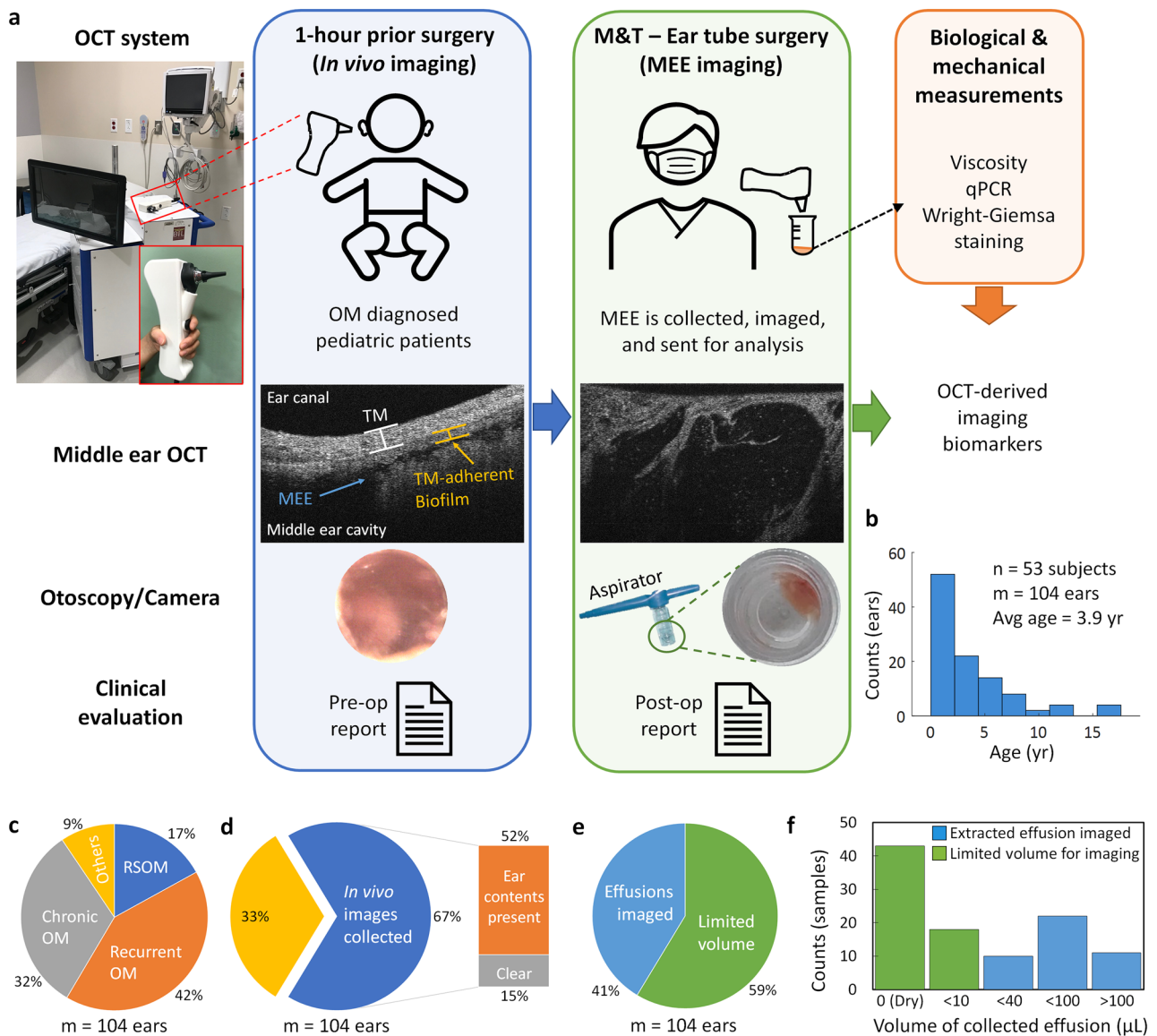


Fig. 1 Study overview — human subject imaging and MEE sample handling. **a** Study design illustrating pre-operative and post-operative imaging with representative OCT and otoscopic images. **b** Age distribution of the subjects. **c** Clinical diagnosis of the subjects per ear. **d** Pre-operative in vivo OCT collection. **e** Post-operative OCT collection of the extracted MEEs. **f** Distribution of sample volume of the

extracted MEEs, where green indicates scant volume or dry. M&T: myringotomy with tympanostomy tube placement, MEE: middle ear effusion, pre-op: pre-operative, post-op: post-operative, qPCR: quantitative polymerase chain reaction, and RSOM: recurrent suppurative otitis media

Handheld High-Resolution Optical Coherence Tomography for Middle Ear

A custom-built, portable, handheld spectral-domain OCT system was employed in the study. The system integrates standard video otoscopy and OCT in a handheld probe. A superluminescent diode (T-860HP; Superlum, Carrigtwohill, Ireland) with a center wavelength of 860 nm and a full-width-half-maximum (FWHM) bandwidth of 130 nm was utilized, providing an axial and lateral resolution of

3.1 µm and 20 µm, respectively. A spectrometer (Cobra-S 800; Wasatch Photonics, Morrisville, NC) with a 4096-pixel line scan camera was used to generate an imaging depth of approximately 2.9 mm at an A-scan rate of 32 kHz. A microelectromechanical (MEMS) mirror (MTI-MZ; Mirrorcle Technologies, Richmond, CA) was used to provide a lateral scanning range of approximately 2.5 mm. Simultaneous camera imaging (MU9PC-MH; XIMEA, Münster, Germany) was performed to visualize the TM as in standard otoscopy and to provide guidance while collecting OCT

images. Detailed schematics of the OCT system can be found in previous publications [26].

Quantitative Metrics for Middle Ear OCT Images

The OCT images were semi-automatically segmented to detect the TM and TM-adherent biofilm, as well as the MEEs, after the OCT images were median filtered and thresholded by the normalized image intensity (Fig. 3). The thickness of the TM was computed assuming a refractive index of 1.44 [27]. Next, a binary mask to select the TM, TM-adherent biofilm, and MEEs was generated, and the relative fluid level was measured using the segmented MEEs. The ratio of the selected binary mask for the MEEs to the overall imaging depth in OCT was calculated to determine the relative fluid level as a percentage (%). As the image can be located at a slightly different depth, a total of 700 pixels in depth was arbitrarily chosen to represent the overall middle ear cavity that can be visualized with OCT for all images.

Texture analysis to assess the intensity distributions of the MEEs was performed on regions of interest (ROI). Each ROI had a width of 150 pixels and a length of 100 pixels in size, equivalent to around 600 μm by 290 μm (width by depth). The raw intensity distribution (before log-compression) within the ROI was fitted to the gamma distribution, described by the following:

$$f(x, \alpha, \beta) = \frac{1}{\Gamma(\alpha)} \beta^\alpha x^{\alpha-1} e^{-\beta x} \quad (1)$$

where alpha and beta represent the shape and scale parameter, respectively. The ratio ($\frac{\alpha}{\beta}$) was computed and used to represent the effective tissue scatterer density within the ROIs [28, 29]. As the ROI was spatially moved across lateral regions in each B-scan, the mean ratio of $\frac{\alpha}{\beta}$ was calculated.

The estimated attenuation coefficient was computed along each A-scan, and a pseudo-color map was generated. The optical attenuation coefficient was estimated by [30]

$$\mu[i] \approx \frac{I[i]}{2\Delta \sum_{i+1}^{\infty} I[i]}, \quad (2)$$

where I denotes the signal intensity, and Δ indicates the pixel size. OCT-derived metrics (texture analysis and estimated optical attenuation coefficients) were calculated for both in vivo and extracted MEEs. An additional metric, named a pocket ratio, was developed to represent the ratio of more low-scattering components (clear fluid or trapped air) of the extracted MEEs. For example, MEEs observed with OCT are highly heterogeneous, containing different ratios of scattering and more transparent components. The pocket ratio was calculated by thresholding the estimated attenuation coefficients. A total of 200 pixels in depth from the top boundary of the extracted MEEs was selected as a ROI (Fig. 3b). Then, a binary mask was

generated to convert and compute a ratio of the pocket (more transparent region) to the selected region of interest. It is hypothesized that the lower pocket ratio indicates a thicker MEE with a greater amount of mucus.

Mechanical Viscosity Measurement

On the day of the biological and mechanical measurements, the MEE samples were thawed at room temperature. For MEE volumes greater than 70 μL , the viscosity of the MEE samples was mechanically measured at room temperature (22 $^{\circ}\text{C}$) using a commercial rheometer (Merlin VR, Rheosys, Princeton, NJ), under a biosafety cabinet. Measurements at 26 revolutions per minute (rpm) using the 2-degree cone/plate following the manufacturer's protocol were used. The viscosity was calculated from shear stress and shear rate using the provided software (MICRA, Rheosys, Princeton, NJ). No significant difference in the measured viscosity of the MEEs was expected from one cycle of freezing to -80°C and thawing, as a previous study with mucoid, mucopurulent, and purulent sputum showed that the degradation of the mechanical viscosity measurement can be prevented by freezing and storage at -70°C [31]. Since the higher temperature results in a lower viscosity, the viscosity of the extracted MEEs measured at 22 $^{\circ}\text{C}$ may overestimate the viscosity of the MEEs present in the middle ear cavity. The viscosity was not measured at body temperature ($\sim 37^{\circ}\text{C}$) in this study to prevent evaporation and dehydration of the samples that already comprised a small volume.

Bacterial Load From Quantitative PCR

When the total volume of the sample was greater than 50 μL , DNA in the MEE was extracted and purified from a 50- μL aliquot of the MEE samples using a commercial QIAamp UCP Pathogen mini kit, following the manufacturer's protocol. Genomic DNA of one of the OM-causing strains, *Pseudomonas aeruginosa* (ATCC 49619, Manassas, VA), was extracted from overnight cultures using the QIAamp UCP Pathogen mini kit for calibration purposes. DNA concentrations and purities were determined with a spectrophotometer (GeneQuant 1300, GE Healthcare Life Sciences, Piscataway, NJ).

Total bacterial loads were determined using a universal bacterial primer [32]. The forward (5'-TCCTACGGGAGG CAGCAGT-3' at 300 nM) and the reverse (5'-GGACTA CCAGGGTATCTAATCCTGTT-3' at 300 nM) primers were used. Purified DNA of *P. aeruginosa* in the range of 200 fg to 2000 ng was used to standardize the measurements. Quantitative PCR (qPCR) was performed with a commercial QuantStudio 7 Flex system (Applied Biosystems, Waltham, MA) using 384-well plates in a reaction volume of 20 μL

using Power SYBR Green PCR Master Mix (Thermo Fisher, Waltham, MA). The conditions across all sample measurements were 50° for 2 min and 95° for 10 min, followed by 40 cycles of amplification at 95° for 15 s and 60 °C for 1 min. The software supplied by Applied Biosystems was used to analyze qPCR data. The reactions were triplicated, and the mean values were determined.

Wright-Giemsa Stain on MEE Smears

When the volume of the MEE sample was not sufficient for DNA extraction (< 50 µL) and viscosity measurement (< 70 µL), or when the remaining MEE sample after aliquoting for the DNA extraction and viscosity measurement was available, Wright-Giemsa staining (#9990710; Thermo Fisher Scientific, Waltham, MA) was performed on MEE smears to visualize immune cells, bacteria, and mucus in the effusion by differential staining. The slides were examined under a standard brightfield microscope (Zeiss Axio Observer D1; Zeiss, Oberkochen, Germany).

Statistical Method

All statistical analysis was performed in MATLAB R2017b (MathWorks, Natick, MA). A two-tailed Student's *t*-test was used to compare the means of the measurements in two groups. For comparing the means of measurements in more than two groups, a one-way analysis of variance (ANOVA) with a multiple comparison test was performed. The Tukey's honestly significant difference (HSD) test was performed to further examine which specific groups were significantly greater or less than one another, after ANOVA statistics detected a significant effect ($p < 0.05$). A significance level (α) was set at 0.05 for all statistical analysis.

Results

A graphical overview of the study is illustrated in Fig. 1. A total of 53 pediatric subjects (104 ears, average age of 3.9 years; 49% male) undergoing M&T were recruited for this study. Clinical diagnoses of the subjects include various subtypes of recurrent and chronic OM, such as chronic OM with effusion (chronic OME), recurrent acute OM (RAOM), and recurrent or chronic suppurative OM (persistent ear discharge) without rupture [1]. RAOM is defined by at least 3 episodes of acute OM (AOM) in 6 months or at least 4 episodes in 12 months with 1 or more episode in the previous 6 months [1, 9]. In vivo middle ear OCT was collected ~ 1 h prior to the M&T in the pre-operative room from 70 ears out of 104 ears (67%). All subjects were awake and sitting on a chair during OCT imaging. Some subjects were not able to be imaged with OCT because (in order of decreasing

frequency): (1) parents or legal guardians only agreed to provide the collected samples, not imaging prior to the M&T; (2) subjects were not tolerant of otoscopic imaging as determined by parents or legal guardians, physicians, or research coordinators; and (3) delayed clinic schedules did not allow additional time for pre-operative imaging. Out of 67% (70 ears) in which pre-operative OCT images were collected, 15% (16 ears) had dry ears, determined by the surgeons who performed the M&T. The fresh, extracted MEE samples were received immediately after M&T and imaged using the same OCT instrument from 43 ears out of 104 ears (41%). MEE samples were not collected from the remaining 61 ears either because they were dry (43 ears), or the MEE samples were too thick (glue ear) and/or scant (18 ears) to be extracted from the thin suction tube.

OCT Atlas of Middle Ear Conditions During OM

While individual middle ear conditions and compositions of the MEEs may vary, quantitative structural information of the MEEs can help in generating a new way of characterizing the state of the diseases regarding the properties of the MEEs. Figure 2a–c show representative OCT images of the middle ear conditions prior to the M&T. The presence of the TM-adherent biofilm (ranging from 50 to 200 µm thick in Fig. 2a, c), the air-MEE boundary, and different textures and features of the MEEs can be assessed and visualized. Under OCT, serous MEEs are characterized by more particulate-like scattering features in a darker background, whereas mucoid MEEs are presented with more uniform and densely scattering materials. The air-MEE boundary is hypothesized to correlate with relative fluid volume. For example, the middle ear in Fig. 2a may contain serous MEE and have less fluid volume than those in Fig. 2b, c. Standard otoscopy (bottom right insets) cannot provide the same level of detailed visualization and quantitative information for the middle ear contents behind the TM.

To better appreciate the broad range of the MEEs observed across these 70 ears, an atlas of in vivo middle ear OCT was generated. In Fig. 2d, the horizontal axis indicates the relative fluid level (volume) of the MEEs from scant to filling, whereas the vertical axis represents the relative optical turbidity that can categorize the MEEs, from serous to mucoid type. Varying sizes of particulate features in the serous MEEs are also shown (white arrowheads), and different morphologies of the TM-adherent biofilms are highlighted by yellow arrowheads in Fig. 2d.

Development of Quantitative OCT Metrics

Figure 3 describes the custom-developed OCT metrics for the in vivo middle ear and the extracted MEEs. The binary mask to select the TM, TM-adherent biofilm, and MEE

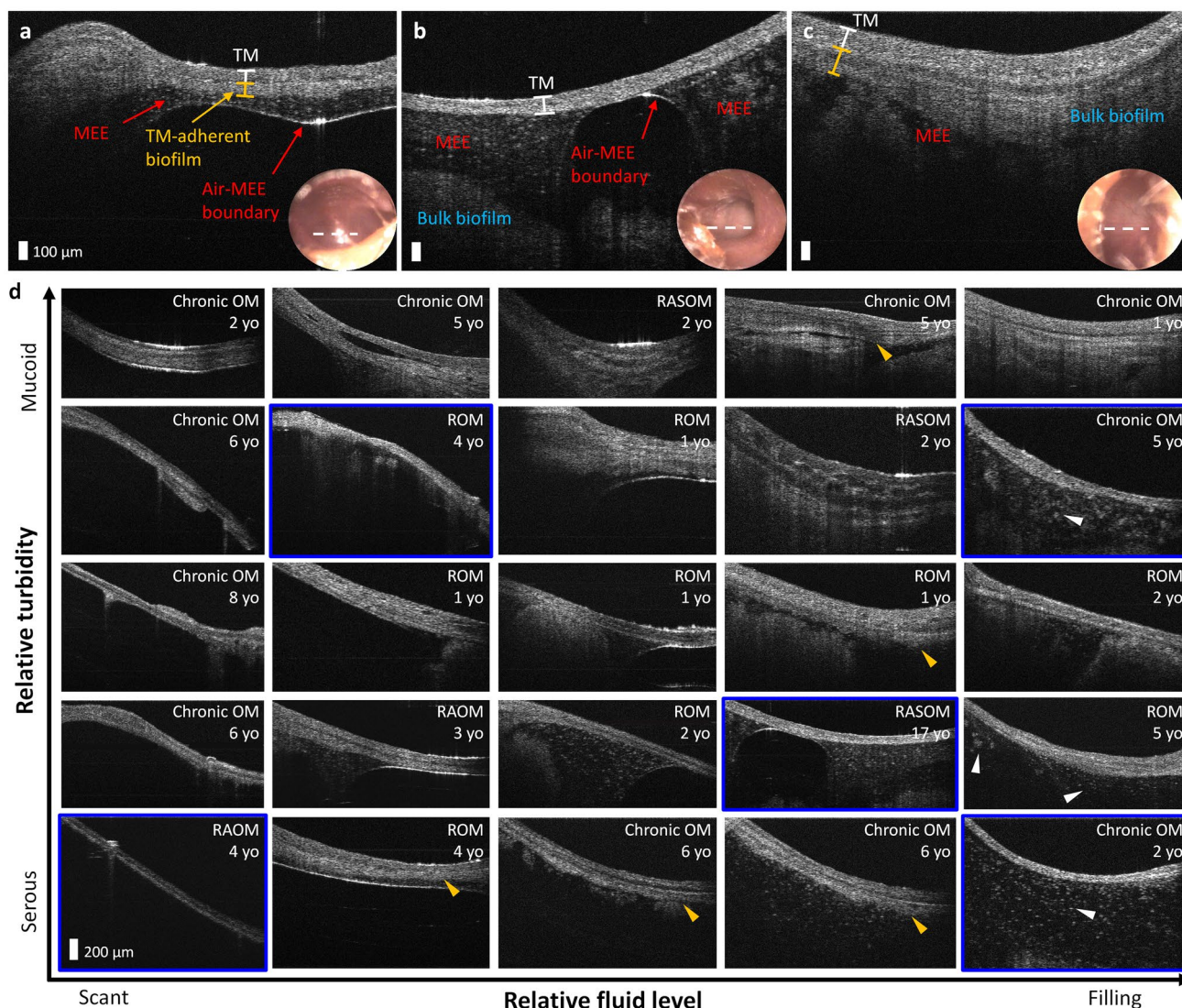


Fig. 2 OCT atlas of middle ear conditions in recurrent and chronic OM. Representative OCT and otoscopy (bottom right inset) of **a** 4-year-old female diagnosed with recurrent OM (ROM), **b** 17-year-old female diagnosed with recurrent acute suppurative OM (RASOM) without rupture, and **c** 1-year-old female diagnosed with chronic OM with mucoid effusion (OME). The white dotted line on the otoscopy surface image indicates the scanning region of OCT. **d** Middle ear OCT atlas of OM. Clinical diagnoses and subject ages are shown in the top right corner of

each image, and the blue framed images indicate that no obvious boundary of the TM-adherent biofilm is visualized with OCT. Yellow arrowheads indicate varying thickness of TM-adherent biofilms, and white arrowheads show different sizes of particulate features in the serous MEEs. TM: tympanic membrane, MEE: middle ear effusion, ROM: recurrent OM, and RAOM: recurrent acute OM

was generated based on the normalized image intensity and depth profiles. The relative fluid level (%) was calculated using the ratio of the binary mask in depth to the partial middle ear cavity that can be visualized with OCT. Next, texture analysis (α/β) was performed in selected regions of interest by fitting the OCT intensity distribution to a gamma distribution. The estimated optical attenuation was computed to examine the signal decay along the depth [30], which can be used to assess the reflectivity and heterogeneity of the optical scattering properties. While

the MEE is generally categorized into serous and mucoid type in the current clinical management of OM, OCT of the extracted MEEs revealed a third category ('combined' type), containing optical properties of both the serous and mucoid MEEs. A pocket ratio represents the ratio of more transparent components (i.e., water) within the MEEs, compared to more dense materials (i.e., mucus). A lower pocket ratio (%) indicates a higher content of optically dense materials, such as mucus and biofilm, and high homogeneity of the sample.

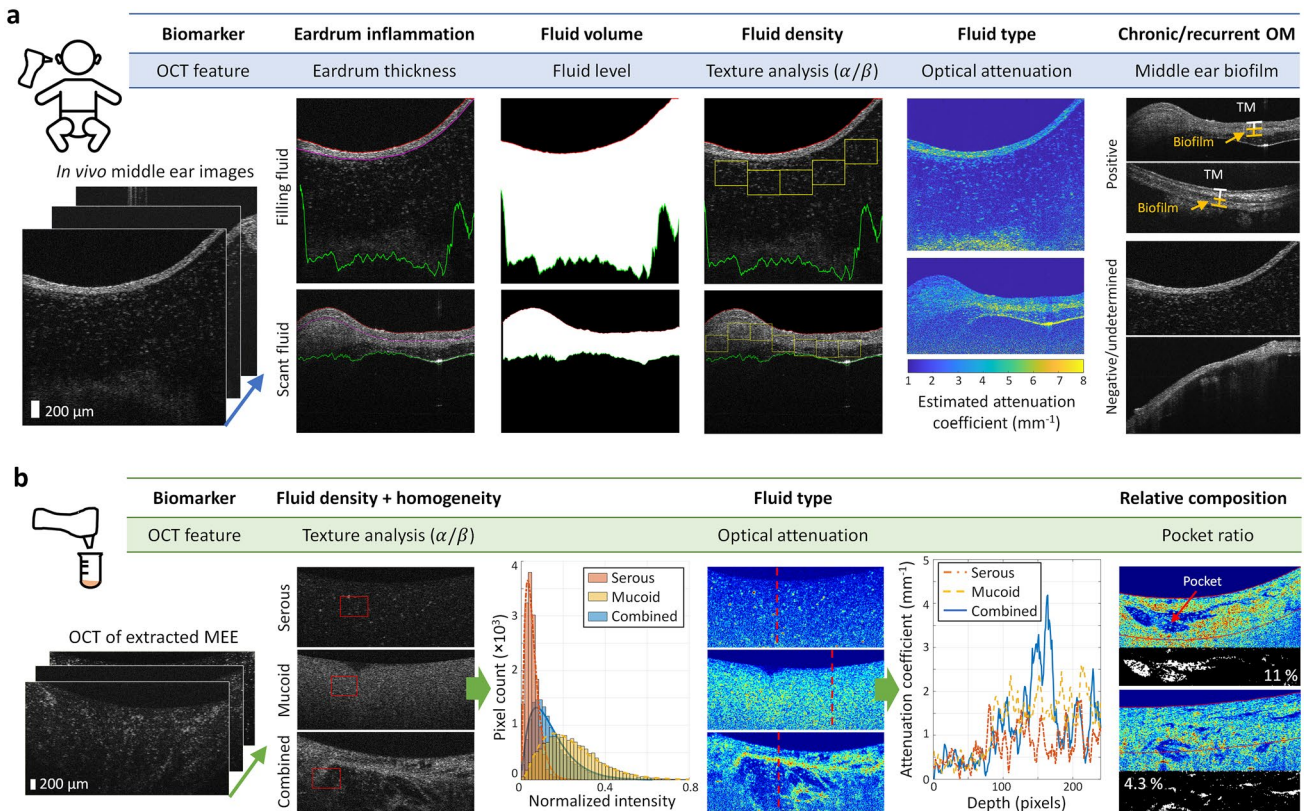


Fig. 3 Illustration of the OCT-derived quantitative metrics in the middle ear. The left-most column indicates representative OCT of **a** in vivo middle ear and **b** extracted MEE. Each OCT feature is indicated and linked to the potential biomarker in OM. In **b**, regions of interest (red box) in the MEEs are shown for serous and mucoid types of the MEEs,

where the texture analysis was performed by fitting distributions of the normalized intensity. The estimated optical attenuation coefficient was calculated and pseudo-colored to highlight different types of the MEEs, and to indicate the pocket ratio in the extracted MEEs

In Vivo Optical Middle Ear Characterization

To determine the diagnostic feasibility of non-invasive OCT imaging prior to M&T, the quantitative OCT metrics were correlated with the pre-operative diagnosis and post-operative reports. The optical attenuation coefficient was the most effective parameter for statistically differentiating the serous from the mucoid MEEs ($p=0.0015$ based on pre-operative diagnosis and $p=0.0004$ based on post-operative report, in Fig. 4a). There were four cases (ears) pre-operatively diagnosed with serous OM, but mucoid MEEs were identified during the M&T. Interestingly, OCT of these four cases showed the presence of serous-like MEEs near the TM (anteriorly, yellow arrows in Fig. 4), whereas a thicker substance was found >0.5 mm deeper (posteriorly, white arrows in Fig. 4) inside the middle ear cavity. This may explain the discordance between pre-operative diagnosis and surgical interpretation of the MEEs, and reaffirms the diagnostic challenge using otoscopy-based methods due to the lack of depth-resolved visualization. We believe that the thicker substance (white arrows) is likely the bulk biofilm biomass, which can build up and move around in the middle ear cavity as the disease

progresses. In addition, this suggests that the in vivo middle ear contents can be highly heterogeneous, where sub-categorization of MEE types might be beneficial. The ears with bilateral OM often exhibited similar OCT characteristics of the middle ear contents, as expected, with an example shown in Fig. 4c. The thickness of the TM-adherent biofilm was greater with the presence of mucoid MEEs than with serous MEEs, with a marginal significance ($p=0.0407$). The thicknesses of the TM-adherent biofilm and the TM were not statistically correlated within the type of chronic OM (i.e., recurrent acute suppurative OM compared to chronic OM), while a previous study [13] showed significant differences in the overall thickness of the TM when comparing chronic OM to that of normal ears and ears with acute OM.

Next, the fluid level (%) non-invasively estimated from OCT was correlated with the fluid volume described in the post-operative reports (dry, scant, and filling MEEs) and shown in Fig. 4e. Note that this study was not designed as interventional so surgeons were not informed of this estimate prior to surgery, and the surgeons may perform and surgeons may perform myringotomy for short-term ventilation of dry middle ears. The OCT-estimated fluid levels in

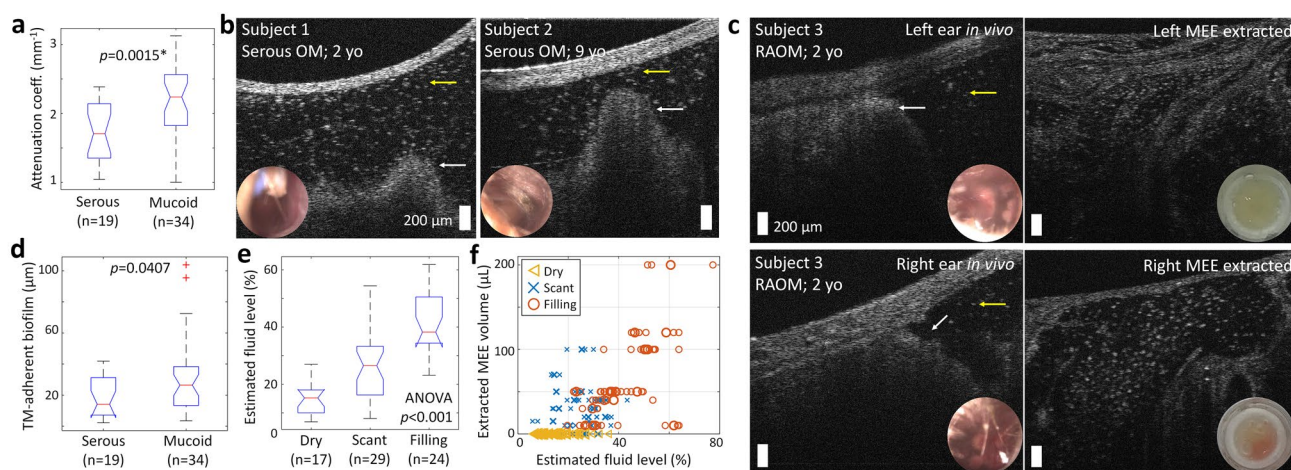


Fig. 4 Comparison of the quantitative OCT parameters from the in vivo middle ear and the clinical evaluations. **a** Comparison of the estimated optical attenuation coefficient between serous and mucoïd MEEs following pre-operative diagnosis. *When following post-operative report, $p=0.0004$. **b** OCT of pre-operatively diagnosed with serous OM, but mucoïd MEEs were post-operatively identified. Yellow arrows indicate serous-like MEEs, whereas white arrows indicate bulk tissue-like materials. **c** Subject with bilateral recurrent acute OM (RAOM) showing similar heterogeneous characteristics of the MEEs between

right and left ears. Bottom right insets represent otoscopy and standard digital camera view of the TM and the extracted MEE, respectively. **d** Comparison of the TM-adherent biofilm thickness between ears with serous and mucoïd MEEs. **e** The estimated fluid level compared with the post-operative report. **f** Plot of the measured MEE volumes after the M&T with the estimated fluid level from in vivo OCT. The larger, bold markers indicate the averaged OCT metrics from three representative OCT B-scans from each ear, whereas the smaller markers indicate OCT metrics from each OCT B-scan

these groups were statistically different ($p < 0.0001$), where the scant group showed a statistically higher estimated fluid level than that of the dry group, while showing a statistically lower estimated fluid level than that of the filling group. The estimated fluid level was also compared with the measured fluid volume (μL) of the collected MEEs, as shown in Fig. 4f. Note that the entire MEE volume may not have been aspirated during M&T, and it was not practical to non-destructively recover the entire sample content from the suction trap after the M&T. Nonetheless, these results suggest that the cross-sectional OCT B-scans may provide a means to non-invasively estimate the relative MEE volume.

Optical Characterization of the Extracted Middle Ear Effusions

Immediately after M&T, the extracted MEEs were imaged using the same OCT system as well as a standard smartphone camera (iPhone7, Apple, Cupertino, CA). The OCT of the extracted MEEs revealed more comprehensive information than in vivo OCT, as direct optical measurement of the MEE was possible without the TM and without the spatial and angular dependence of the probe imaging in the ear canal, which can decrease the signal-to-noise ratio (see Fig. 4c). However, the extracted MEEs no longer represent the in vivo conditions in the middle ear due to the surgical aspiration procedure. Representative OCT images indicating each type of the extracted MEEs are shown in Fig. 5a.

The serous MEE group was determined based on the post-operative interpretations of the extracted MEEs by the surgeons. The remaining datasets were all described as mucoïd type on the surgical report; however, these datasets were further divided into the mucoïd (homogeneous, likely mucus) and combined (heterogeneous containing both serous- and mucoïd-like features) types. The serous MEEs were the least common type in this study, and were found from the statistically older pediatric subjects (Fig. 5c). These findings agree with a previous study [33]. In Fig. 5d, the custom-developed OCT metrics of the three MEE types are plotted. The larger, bold markers indicate the averaged OCT metrics from three representative OCT B-scans from each ear, whereas the smaller markers indicate the OCT metrics from each OCT B-scan. The averaged OCT metrics were used for the statistical analysis because the middle ear contents can be heterogeneous in the middle ear cavity. The statistical analysis revealed that the estimated attenuation coefficient ($p=0.008$) and the pocket ratio ($p=1.32e-04$) can differentiate the serous from non-serous MEE type, and the pocket ratio can further distinguish the mucoïd MEE from the combined MEE type ($p=4.05e-04$; Fig. 5e).

OCT to Estimate Relative Viscosity of Effusions

Since the clinical interpretations of the MEE types (serous and mucoïd) are associated with the relative viscosity, mechanically measured viscosities of the extracted MEEs

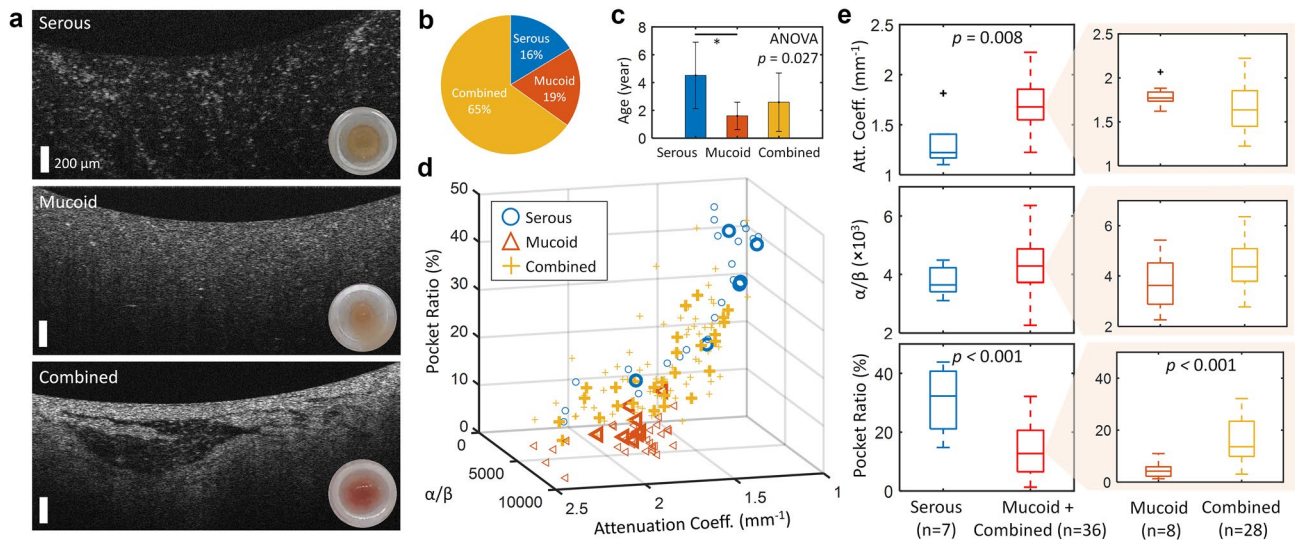


Fig. 5 Three different subtypes of extracted MEEs from the M&T. **a** Representative OCT of the extracted MEEs observed immediately after the M&T. Bottom right insets show standard camera photographs. The distribution of **b** the collected MEE types and **c** the subject age in each MEE type. **d** The custom-developed OCT metrics are

plotted for different types of the MEEs. Larger, bold markers indicate averaged metrics from three representative OCT B-scans in each ear, whereas smaller markers are plotted from each OCT B-scan. **e** Statistical comparison of each OCT metric in MEE subtypes

were compared with the OCT-derived parameters. The number of samples was limited because not every extracted MEE resulted in sufficient volume (> 70 µL) for the mechanical viscosity measurement. Thus, the extracted MEEs were divided into more mucoïd ($n = 10$) and less mucoïd ($n = 2$) groups using a thresholding viscosity (1000 cP) that can statistically separate the two groups. All samples included in this analysis were categorized as the combined type. The OCT-derived metrics, particularly the pocket ratio and the estimated attenuation coefficient, were able to statistically differentiate the viscosity group. This is likely because the two parameters are more sensitive in detecting differences between optically transparent and dense materials, which may also contribute to the differences in the mechanical viscosity.

The estimated optical attenuation coefficients from both in vivo and extracted MEEs were available from 23 ears, and were compared between the MEE types (serous and mucoïd) determined by the post-operative reports, shown in Fig. 6c. A similar trend of higher attenuation coefficients in mucoïd MEEs was found, suggesting that this metric may be sensitive to OCT acquired from both in vivo middle ear and extracted MEEs. However, one case (yellow arrow) containing the scant serous MEE in vivo showed the additional bulk materials in the extracted MEEs, which resulted in greater optical attenuation coefficient from the extracted MEEs.

Wright-Giemsa staining was performed with the remaining MEE. The smeared and stained effusion samples were inspected under a standard brightfield microscope, and the OCT of in vivo middle ear and the extracted MEEs were

compared, as shown in Fig. 6d. The stained images indicate the presence of various immune cells (green arrow) and mucus (blue arrow), as well as clusters of bacteria (red arrow). While OCT cannot provide the specific, biochemical information on different components in the MEEs, high structural similarities in OCT and Wright-Giemsa-stained images might explain why the OCT-derived parameters are relevant to the clinically meaningful properties, such as viscosity.

Next, total bacterial loads in the extracted MEE samples were compared with the OCT-derived parameters. It was hypothesized that the dense, uniform textures of the MEEs, indicated by the greater α/β ratio from the texture analysis, will indicate high mucus content with less bacteria present. However, while a few samples followed this hypothesis, the OCT parameters were not statistically correlated with the measured amount of bacterial DNA in all samples. This is not entirely unexpected because a single bacterium and small clusters of bacteria in highly heterogeneous samples are not resolvable with the current system resolution of OCT.

Proposed Decision Tree Using Middle Ear OCT Images

Based on the wide variety of in vivo middle ear OCT images and the capability of generating quantitative information on MEEs, a decision tree is proposed in Fig. 7. To reflect the current clinical guidelines [3, 9, 34, 35], the OCT images are first divided using the presence or absence of a MEE. The middle ear conditions can then

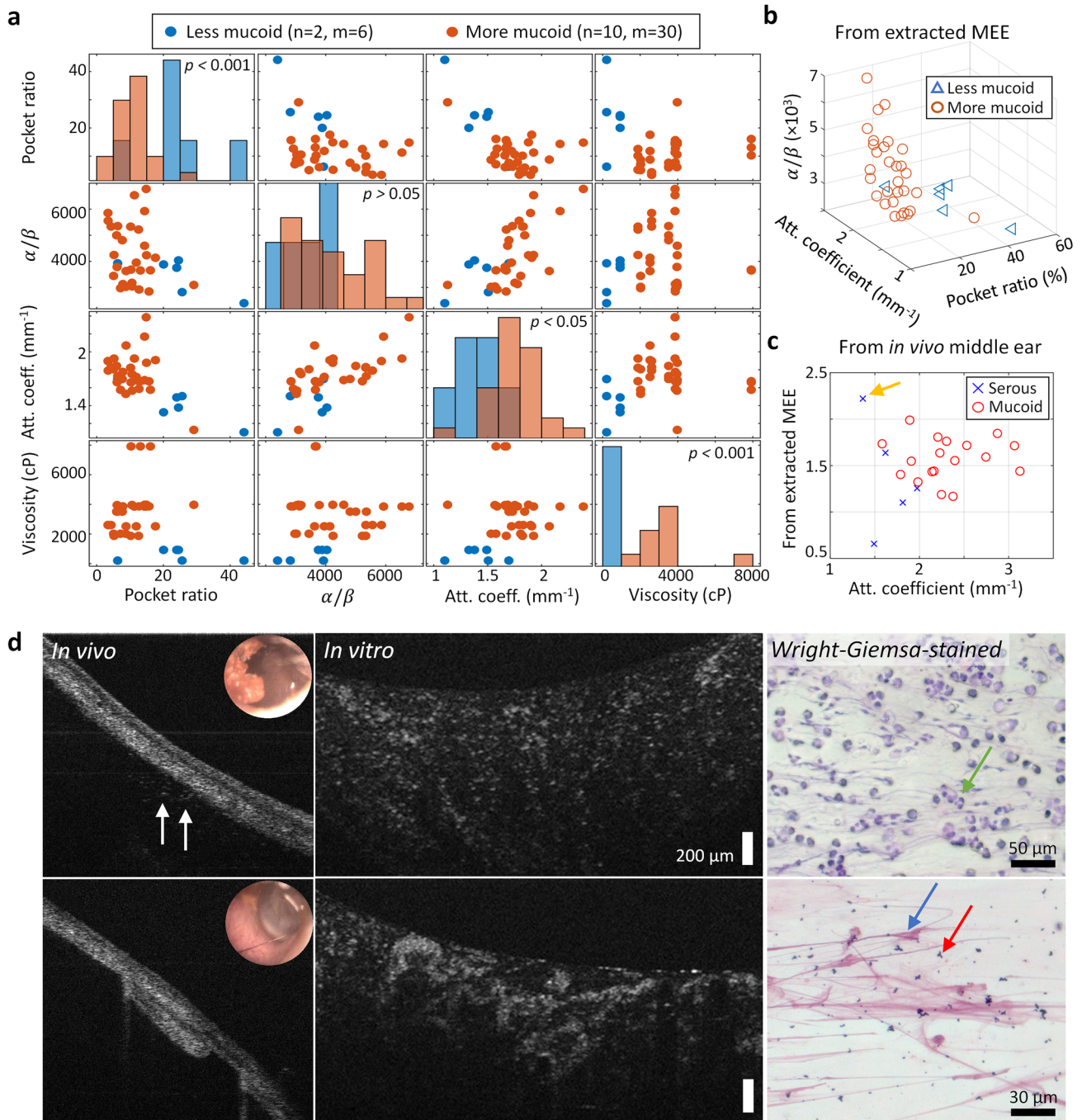


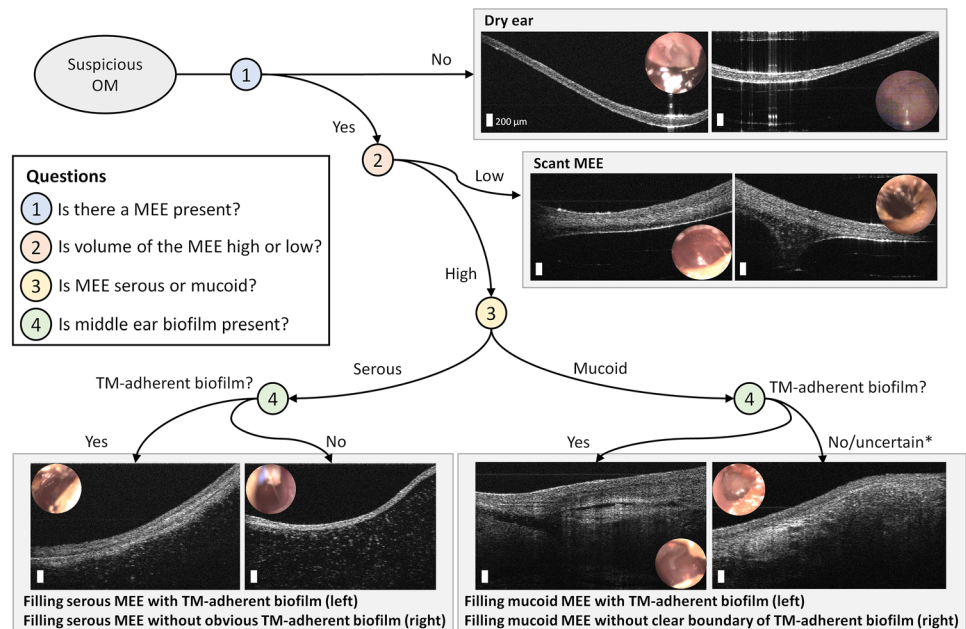
Fig. 6 OCT-derived parameters correlated with mechanically measured viscosity and clinical interpretation of the MEEs. **a** Correlation map of the three OCT-derived parameters with the measured viscosity group. **b** Plot of the OCT-derived parameters from OCT of the extracted MEEs. **c** Plot of the estimated attenuation coefficients calculated from the *in vivo* OCT and OCT of the extracted MEEs. Yellow arrow shows an outlier where *in vivo* OCT did not show addi-

tional bulk materials located deeper in the middle ear cavity, and thus showing greater attenuation coefficient from the extracted MEEs. **d** Comparison of *in vivo* OCT, OCT of the extracted serous MEE, and Wright-Giemsa-stained MEE. White arrows indicate the presence of serous MEE in OCT, and green, blue, and red arrows show immune cells, mucus, and cluster of bacteria, respectively

be subdivided into scant and filling MEEs, determined by the air-MEE boundary in the depth-resolved OCT images. Next, the MEEs can be divided into serous or mucoid

types. Lastly, the presence of a TM-adherent biofilm can be considered, which may indicate a more chronic state of OM.

Fig. 7 A decision tree of middle ear OCT during OM, depending on the presence of a MEE, relative fluid level, type of MEE, and biofilm. *It may be less likely not to have any TM-adherent biofilm with filling mucoid MEE



Discussion

In this study, varying presentations of OM-related middle ear contents were captured in vivo and assessed using the custom-developed, handheld OCT system and algorithms to correlate optical images with clinically validated information. Among 104 ears from 53 subjects (average age of 3.9 years), in vivo imaging was performed on 70 ears (67%), and the effusions from 54 ears were analyzed using OCT images. When MEEs were identified, the presence of a TM-adherent biofilm was identified from most ears (89.6%). The estimated optical attenuation coefficients from OCT images differentiated the types of MEEs, which showed agreement with surgical interpretation of the MEEs.

Previous studies have biologically characterized the extracted MEEs after M&T to understand the pathogenesis, recurrence, and susceptibility of otopathogens responsible for OM. For example, studies have shown that serous MEE may indicate shorter duration of OM than mucoid MEE [36], and may correspond to better medical outcomes than mucoid MEE [37]. The capability of estimating the fluid volume may help determine treatment strategies, as the greater volume will affect hearing, indicating immediate interventions [38, 39], and may be associated with the recurrence rate after M&T [40]. Nevertheless, physicians currently do not have sufficient access to such information, and thus integrating the above research findings into clinical practice is challenging. Furthermore, the presence of middle ear bacterial biofilms has been identified in recurrent acute OM (RAOM), chronic OM, and chronic OM with effusion (COME) [22–25], while comprehensive understanding of biofilm-related pathogenesis for different subtypes of OM is

still largely unknown, partly due to the lack of non-invasive detection techniques that can enable in vivo and longitudinal investigations. Thus, the ability to directly examine in vivo MEE and biofilm characteristics demonstrated in this study will facilitate understanding of the heterogeneous MEE types and their impacts on the medical outcomes of OM, leading to personalized clinical management and biofilm-related in vivo research investigations.

Among the subjects who were scheduled for M&T and were identified with the presence of MEEs in in vivo OCT, 89.6% showed the presence of the TM-adherent biofilm, again reasserting the role of bacterial biofilms in chronic and recurrent OM. In addition, this number is likely underestimated because only the biofilm adhered to the TM was considered, as determined by OCT. The presence of the TM-adherent biofilm was not biologically validated in this study; however, our previous studies have confirmed that the thin, highly scattering layer adhered to the TM, which can be detected by OCT, is bacterial biofilm [18, 41]. While no statistical relationship between the OCT-derived parameters and the total bacterial load in MEEs was found, similarities between the OCT and Giemsa-stained MEE images imply that OCT has the potential to non-invasively provide detailed structural characteristics of the MEEs containing various immune cells, mucus, and biofilm.

One major strength of this study is the correlation between in vivo middle ear OCT acquired 1 h prior to M&T and OCT of the freshly extracted middle ear contents. Quantitative analysis showed that the in vivo middle ear OCT metrics exhibited high correspondence with the post-operative assessment of the MEEs, suggesting that in vivo OCT data, which captures microstructures adjacent to the TM and a

few millimeters behind, can be representative of the MEEs in the middle ear cavity. Compared to otoscopy-based estimation of air-fluid level, quantifying the relative fluid level using OCT will offer an additional dimension of the MEEs in depth and other optical scattering characteristics. Over time, with acquisition of additional data, the OCT device will be able to provide a useful grading system [40] that assesses the likely viscosity, quantity of fluid, and degree of biofilm. With additional clinical studies, this grading system can further be linked to patient outcomes and help predict which patients are more likely to benefit from M&T placement, and which patients may more likely resolve their MEE with a period of watchful waiting. A follow-up study to investigate the long-term outcomes of the combined MEE type compared to the mucoid MEEs in chronic and recurrent OM is ongoing.

There are several challenges that need to be discussed for future studies. First, the limited volume of the extracted MEEs made it challenging to measure mechanical viscosity and bacterial load. A microfluidic device that can measure viscosity may be an alternative option for smaller volumes of MEEs. Second, the limited imaging depth of OCT may not represent the entire middle ear cavity. Development of high-speed, long-range, swept-source-based OCT at longer wavelengths that enable real-time volumetric imaging of the middle ear will be beneficial for many clinical imaging studies, including longitudinal investigations, and to visualize a greater extent of the ossicles and mucosa deeper in the middle ear cavity. Though blood-dominated MEE samples were excluded, the presence of blood from M&T might have affected the measurements with the extracted MEEs. Lastly, a greater number of subjects with serous MEEs is needed. In the future, quantitative metrics will benefit from machine learning-based approaches [16, 17] to further characterize middle ear content and interpret the OCT images. In addition, our recent studies [42, 43] combining OCT with Raman spectroscopy (RS-OCT) has shown promise for differentiating bacteria-based OM from viral OM, which can further impact the clinical decision-making process.

With development of low-cost and compact OCT devices, OCT can be utilized as a longitudinal imaging tool to monitor OM progression and treatment response [19, 41]. While not yet considered in the clinical management of OM, the extended information about the middle ear contents (subtypes and relative volume of MEEs and TM-adhered biofilm) can potentially help clinical management in the future, and may dramatically improve the diagnostic tools available in Pediatric, Primary Care, and ENT clinics. For example, understanding and defining the treatment failures of AOM [44] can be quantitatively described by MEE characteristics, in addition to symptoms. Another possibility is to help establish consensus guidelines for M&T in recurrent acute OM [45] by correlating a recurrence rate with the OCT-derived biomarkers in MEEs and middle ear biofilms after M&T

or antibiotic treatment. Overall, this work demonstrated the potential clinical utility of middle ear OCT imaging technology and generated an atlas of middle ear OCT in OM, which will be utilized in future studies to help develop personalized medicine approaches for OM.

Acknowledgements The authors thank MaryEllen Sherwood and Christine Canfield from the Carle Research Office at Carle Foundation Hospital, Urbana, Illinois, for their help with IRB protocol management and subject recruitment. The authors acknowledge the nursing staff in the Department of Otolaryngology at Carle Foundation Hospital and Champaign Surgery Center at the Fields for their help in subject recruitment and clinical assistance.

Funding This work was funded in part by grants from the National Institutes of Health (R01DC019412, R01EB028615, R01AI160671, P41EB031772) and in part by the McGinnis Medical Innovation Fellowship program.

Data Availability The data that support the findings of this study are available upon reasonable request to the corresponding author and under a collaborative research agreement.

Declarations

Conflict of Interest S. A. B. is co-founder and holds equity interest in PhotoniCare, Inc., which is commercializing the use of OCT for middle ear imaging. M. A. N. has equity interest and serves on the clinical advisory board of PhotoniCare, Inc. The remaining authors declare no conflict of interest.

References

- Schilder AGM, Chonmaitree T, Cripps AW et al (2016) Otitis media. *Nat Rev Dis Prim* 2:1–19
- Coker TR, Chan LS, Newberry SJ et al (2010) Diagnosis, microbial epidemiology, and antibiotic treatment of acute otitis media in children: a systematic review. *J Am Med Assoc* 304(19):2161–2169
- Rosenfeld RM, Tunkel DE, Schwartz SR et al (2022) Clinical practice guideline: tympanostomy tubes in children (Update). *Otolaryngol Head Neck Surg* 166(1S):S1–S55
- Bhattacharyya N, Shay SG (2020) Epidemiology of pediatric tympanostomy tube placement in the United States. *Otolaryngol Neck Surg* 163(3):600–602
- Monasta L, Ronfani L, Marchetti F et al (2012) Burden of disease caused by otitis media: systematic review and global estimates. *PLoS ONE* 7(4):e36226
- Tong S, Amand C, Kieffer A, Kyaw MH (2018) Trends in health-care utilization and costs associated with acute otitis media in the United States during 2008–2014. *BMC Health Serv Res* 18(318):1–10
- Rosenfeld RM (2020) Tympanostomy tube controversies and issues: state-of-the-art review. *Ear Nose Throat J* 99(1_suppl):15S–21S
- Harvey M, Bowe SN, Laury AM (2016) Clinical practice guidelines: whose practice are we guiding? *Otolaryngol Head Neck Surg* 155(3):373–375
- Lieberthal AS, Carroll AE, Chonmaitree T et al (2013) The diagnosis and management of acute otitis media. *Pediatrics* 131(3):e964–999
- Pichichero ME, Poole MD (2005) Comparison of performance by otolaryngologists, pediatricians, and general practitioners on an otoendoscopic diagnostic video examination. *Int J Pediatr Otorhinolaryngol* 69(3):361–366

11. Pichichero ME (2003) Diagnostic accuracy of otitis media and tympanocentesis skills assessment among pediatricians. *Eur J Clin Microbiol Infect Dis* 22(9):519–524
12. Nguyen CT, Jung W, Kim J et al (2012) Noninvasive in vivo optical detection of biofilm in the human middle ear. *Proc Natl Acad Sci* 109:9529–9534
13. Monroy GL, Shelton RL, Nolan RM et al (2015) Noninvasive depth-resolved optical measurements of the tympanic membrane and middle ear for differentiating otitis media. *Laryngoscope* 125(8):E276–282
14. Huang D, Swanson EA, Lin CP et al (1991) Optical coherence tomography. *Science* 254(5035):1178–1181
15. Won J, Monroy GL, Huang PC et al (2020) Assessing the effect of middle ear effusions on wideband acoustic immittance using optical coherence tomography. *Ear Hear* 41(4):811–824
16. Won J, Dsouza R, Monroy GL et al (2021) Handheld briefcase optical coherence tomography with real-time machine learning classifier for diagnosing middle ear infections. *Biosensors* 11(5):143
17. Monroy GL, Won J, Dsouza R et al (2019) Automated classification platform for the identification of otitis media using optical coherence tomography. *NPJ Digit Med* 2(1):1–11
18. Monroy GL, Hong W, Khampang P et al (2018) Direct analysis of pathogenic structures affixed to the tympanic membrane during chronic otitis media. *Otolaryngol Head Neck Surg* 159(1):117–126
19. Monroy GL, Pande P, Nolan RM et al (2017) Noninvasive in vivo optical coherence tomography tracking of chronic otitis media in pediatric subjects after surgical intervention. *J Biomed Opt* 22(12):1–11
20. Preciado D, Nolan RM, Joshi R et al (2020) Otitis media middle ear effusion identification and characterization using an optical coherence tomography otoscope. *Otolaryngol Head Neck Surg* 162(3):367–374
21. Monroy GL, Pande P, Shelton RL et al (2016) Non-invasive optical assessment of viscosity of middle ear effusions in otitis media. *J Biophotonics* 10:394–403
22. Post JC (2001) Direct evidence of bacterial biofilms in otitis media. *Laryngoscope* 111(12):2083–2094
23. Hall-Stoodley L, Hu FZ, Gieseke A et al (2006) Direct detection of bacterial biofilms on the middle-ear mucosa of children with chronic otitis media. *J Am Med Assoc* 296(2):202–211
24. Coticchia JM, Chen M, Sachdeva L, Mutchnick S (2013) New paradigms in the pathogenesis of otitis media in children. *Front Pediatr* 1(52):1–7
25. Thornton RB, Rigby PJ, Wiertsema SP et al (2011) Multi-species bacterial biofilm and intracellular infection in otitis media. *BMC Pediatr* 11(1):94
26. Hubler Z, Shemonski ND, Shelton RL, Monroy GL, Nolan RM, Boppart SA (2015) Real-time automated thickness measurement of the in vivo human tympanic membrane using optical coherence tomography. *Quant Imaging Med Surg* 5(1):69–77
27. Van Der Jeught S, Dirckx JJJ, Aerts JRM, Bradu A, Podoleanu AG, Buytaert JAN (2013) Full-field thickness distribution of human tympanic membrane obtained with optical coherence tomography. *J Assoc Res Otolaryngol* 14(4):483–494
28. Tunis AS, Czarnota GJ, Giles A, Sherar MD, Hunt JW, Kolios MC (2005) Monitoring structural changes in cells with high-frequency ultrasound signal statistics. *Ultrasound Med Biol* 31(8):1041–1049
29. Lindenmaier AA, Conroy L, Farhat G, DaCosta RS, Fluerau C, Vitkin IA (2013) Texture analysis of optical coherence tomography speckle for characterizing biological tissues in vivo. *Opt Lett* 38(8):1280
30. Vermeer KA, Mo J, Weda JJA, Lemij HG, de Boer JF (2014) Depth-resolved model-based reconstruction of attenuation coefficients in optical coherence tomography. *Biomed Opt Express* 5(1):322
31. Charman J, Reid L (1973) The effect of freezing, storing and thawing on the viscosity of sputum. *Biorheology* 10(3):295–301
32. Nadkarni MA, Martin FE, Jacques NA, Hunter N (2002) Determination of bacterial load by real-time PCR using a broad-range (universal) probe and primers set. *Microbiology* 148:257–266
33. Val S, Poley M, Anna K et al (2018) Characterization of mucoid and serous middle ear effusions from patients with chronic otitis media: implication of different biological mechanisms? *Pediatr Res* 84:296–305
34. Rosenfeld RM, Shin JJ, Schwartz SR et al (2016) Clinical practice guidelines: otitis media with effusion (update). *Otolaryngol Head Neck Surg* 154(1S):S1–S41
35. Selby M, Wolfram S (2018) Antibiotics for otitis media in children. *Am Fam Physician* 97(12):775A–775B (PMID: 30216004)
36. Matković S, Vojvodić D, Baljosevic I (2007) Cytokine levels in groups of patients with different duration of chronic secretory otitis. *Eur Arch Oto-Rhino-Laryngology* 264(11):1283–1287
37. Dodson KM, Cohen RS, Rubin BK (2012) Middle ear fluid characteristics in pediatric otitis media with effusion. *Int J Pediatr Otorhinolaryngol* 76(12):1806–1809
38. Dai C, Wood MW, Gan RZ (2008) Combined effect of fluid and pressure on middle ear functions. *Hear Res* 236(1–2):22–32
39. Ravicz ME, Rosowski JJ, Merchant SN (2004) Mechanisms of hearing loss resulting from middle-ear fluid. *Hear Res* 195
40. Song C II, Kang BC, Shin CH et al (2021) Postoperative results of ventilation tube insertion: a retrospective multicenter study for suggestion of grading system of otitis media with effusion. *BMC Pediatr* 21(1):1–7
41. Won J, Hong W, Khampang P et al (2021) Longitudinal optical coherence tomography to visualize the in vivo response of middle ear biofilms to antibiotic therapy. *Sci Rep* 11:5176
42. Locke AK, Zaki FR, Fitzgerald ST et al (2022) Differentiation of otitis media-causing bacteria and biofilms via Raman spectroscopy and optical coherence tomography. *Front Cell Infect Microbiol* 12:869761
43. Monroy GL, Fitzgerald ST, Locke A et al (2022) Multimodal handheld probe for characterizing otitis media — integrating Raman spectroscopy and optical coherence tomography. *Front Photonics* 3:929574
44. Marom T, Gluck O, Ovnat Tamir S (2021) Treatment failure in pediatric acute otitis media: how do you define? *Int J Pediatr Otorhinolaryngol* 150(Nov):110888
45. Hoberman A, Preciado D, Paradise JL et al (2021) Tympanostomy tubes or medical management for recurrent acute otitis media. *N Engl J Med* 384(19):1789–1799

Publisher's Note Springer Nature remains neutral with regard to jurisdictional claims in published maps and institutional affiliations.

Springer Nature or its licensor (e.g. a society or other partner) holds exclusive rights to this article under a publishing agreement with the author(s) or other rightsholder(s); author self-archiving of the accepted manuscript version of this article is solely governed by the terms of such publishing agreement and applicable law.